

Unfolding ESIPT in Bis-2,5-(2-benzoxazolyl) Hydroquinone and 2,5-Bis(benzo[d]oxazol-2-yl)-4-methoxyphenol: a Comprehensive Computational Approach

Manoj M. Jadhav¹ · Lydia Rhyman² · Ponnadurai Ramasami² · Nagaiyan Sekar¹

Received: 25 December 2015 / Accepted: 26 April 2016
© Springer Science+Business Media New York 2016

Abstract The photo-physical behaviour of bis-2,5-(2-benzoxazolyl) hydroquinone and 2,5-bis (benzo[d]oxazol-2-yl)-4-methoxyphenol was studied using the Density Functional Theory (DFT) and Time-Dependent Density Functional Theory (TD-DFT). All the possible rotamers were optimized to obtain global minimum optimized structure. The theoretical absorption and emission values of rotamers estimated by using TD-DFT [TD-B3LYP/6–31G(d)] are in good agreement with experimental absorption and emission wavelengths. Based on the absorption values, the contribution of respective rotamer is determined theoretically.

Keywords ESIPT · DFT · TD-DFT · Bis-2,5-(2-benzoxazolyl) hydroquinone · 2,5-di(benzo[d]oxazol-2-yl)-4-methoxyphenol

Introduction

Vital importance has emerged recently in the investigation of compounds exhibiting excited-state intermolecular proton

Electronic supplementary material The online version of this article (doi:10.1007/s10895-016-1816-1) contains supplementary material, which is available to authorized users.

✉ Ponnadurai Ramasami
ramchemi@intnet.mu

✉ Nagaiyan Sekar
nethi.sekar@gmail.com

¹ Tinctorial Chemistry Group, Department of Dyestuff Technology, Institute of Chemical Technology, N. P. Marg, Matunga, Mumbai, Maharashtra 400019, India

² Computational Chemistry Group, Department of Chemistry, Faculty of Science, University of Mauritius, Réduit 80837, Mauritius

transfer (ESIPT) phenomenon [1–5]. Spectral comparison of these compounds to the surrounding environment and a large Stokes-shifted fluorescence is of great interest [6]. A combined experimental and theoretical approach has been utilized to understand the four-level photo physical scheme [7] exemplified in the ESIPT process. ESIPT is photo tautomerization progression which usually involves transfer of the hydroxyl or amino proton to an acceptor such as carbonyl oxygen or nitrogen atom. The hydroxyl proton is more acidic and the acceptor group is more basic in the excited state keto than in the ground state enol [8]. The basic acceptor can receive a proton from the acidic group in extremely fast sub-picoseconds time scale and through delocalization of the positive charge about the heterocyclic ring to form a keto species that has large Stokes-shifted tautomer emission [9]. After the relaxation of the keto form to the ground state, the energetically favoured enol form is regained spontaneously by reverse proton transfer in a non-radiative process, to complete the cyclic four-level scheme. Subsequently, this process gives rise to the transient chemical change from enol to keto tautomer, leading to the transient rotation of the electronic properties such as electron density distribution, energies of electronic states, and dipole moments [10].

Emission from the keto state is attributed to a large Stokes-shift, which provides long-wavelength fluorescence by UV-Visible excitation [11]. Presence of this second red shifted emission makes such compounds appealing, and they find a wide range of applications as laser dyes [12], fluorescent probes [13], photochromic dyes [10], sensors [14], organic electroluminescence optical materials [15], photo-stabilizers [16, 17] as well as in fluorescence recording techniques [18]. The development and photo physical characterization of ESIPT organic compounds is of leading interest [19]. ESIPT is largely characterized by the energy level changes of excited states, and only a small energy barrier or even barrier less

transition is allowed. So far, one of the most investigated ESIPT compounds, because of their proficient ESIPT fluorescence, are 2-(2'-hydroxyphenyl)benzoxazole (HBO) [20] and its analogues. ESIPT based benzoxazole derivatives have been potentially used in the application of medicine as cytotoxic agents [21], HIV reverse transcriptase inhibitors, estrogen receptor agonists, anticancer agents. They have also found application as herbicides, as fluorescent-whitening agent dye [22], in bio-conjugation. Density Functional Theory (DFT) has been comprehensively explored for the ground state geometry optimisation and Time Dependent-Density Functional Theory (TD-DFT) and Configuration Interaction Singles (CIS) for exploring excited state behaviour of ESIPT based benzoxazole compounds.

However, there are very few reports unfolding bis-2,5-(2-benzoxazolyl) hydroquinone [23–28] where two hydroxyl groups are available for the ESIPT phenomenon. Out of these two hydroxyl groups, only one can be a part of keto-enol tautomerism, which leads to the possibilities of various conformers. The existence of more than one conformer can be predicted from complicated nature of UV-Visible absorption spectrum which shows five major absorption peaks. To support our observation we have compared absorption spectra with absorption of bis (benzo[d]oxazol-2-yl)-4-methoxyphenol where one of the hydroxyl proton is replaced by methyl group. This replacement leads to simplified nature of absorption spectrum with three absorption peaks in spite of having more number of possible conformers [23]. The substantial change in number of major peaks in the absorption spectrum upon replacement of one acidic proton by methyl group leads to the curiosity to find out which of the conformers is responsible for the complicated absorption spectrum of bis-2,5-(2-benzoxazolyl) hydroquinone. Therefore, taking into account various possibilities of conformers and their contributions to

absorption spectra and in continuation of our research work on ESIPT based fluorescent materials, herein, we report Time Dependent Density Functional Theory (TD-DFT) explorations to enlighten the geometry of different conformers of bis-2,5-(2-benzoxazolyl) hydroquinone and 2,5-di(benzo[d]oxazol-2-yl)-4-methoxyphenol along with their environmental dependence of absorption and fluorescence maxima.

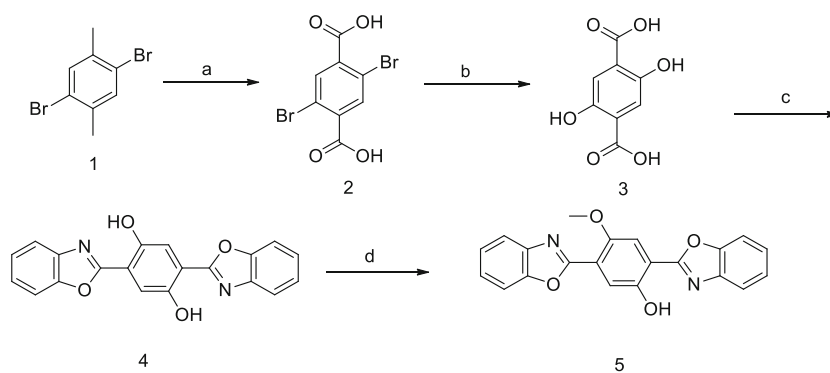
Synthesis Strategy

The preparations of bis-2,5-(2-benzoxazolyl) hydroquinone and its monomethoxy derivative 2,5-di(benzo[d]oxazol-2-yl)-4-methoxyphenol are represented in Scheme 1. 2,5-Dibromo-1,4-dimethylbenzene is oxidized by KMnO_4 , pyridine and H_2O by using modified procedure [29, 30] to get the compound 2. The compound 3 was obtained by treating 2 with Na_2CO_3 in the presence of catalytic amount of pyridine + CuBr complex in H_2O . Compound 3 was heated with 1 eq of 2-aminophenol and 10 eq. PPA to get compound 4 bis-2,5-(2-benzoxazolyl) hydroquinone [24]. It was purified by several crystallization in DMF. Compound 4 on controlled monomethylation with MeI in DMF in presence of NaOH gives 2,5-di(benzo[d]oxazol-2-yl)-4-methoxyphenol [27]. This was further purified by using column chromatography.

Computational Methods

The ground state geometry optimization of the various rotamers and their respective keto tautomers of the compounds 4 and 5 in their C_s symmetry were performed in gas phase and in six different solvents using Density Functional Theory (DFT) [31]. The B3LYP hybrid functional was

Scheme 1 Synthesis of Bis-2,5-(2-benzoxazolyl) hydroquinone (Compound 4) and 2,5-Bis(benzo[d]oxazol-2-yl)-4-methoxyphenol (compound 5)



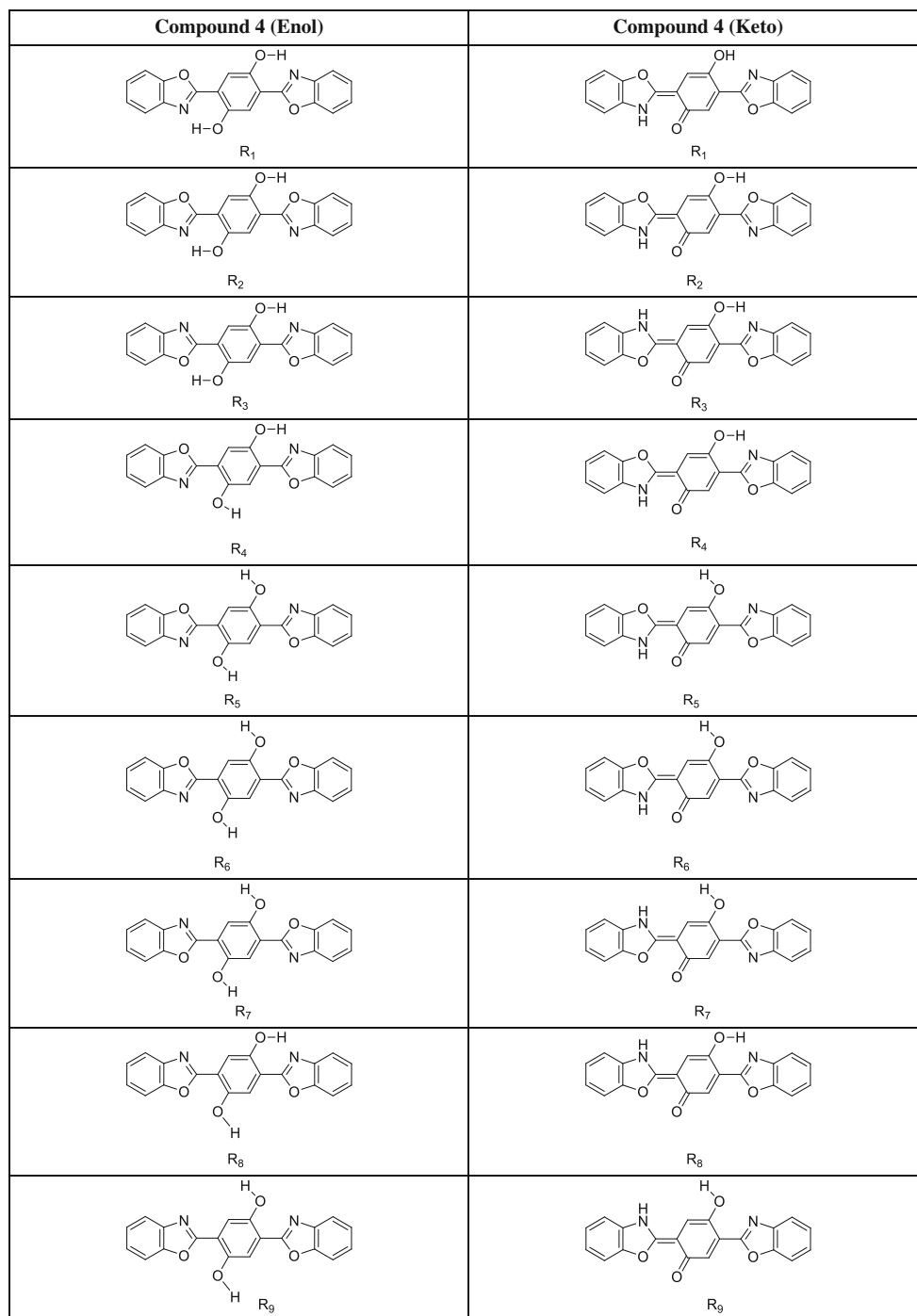
Reaction conditions:

- KMnO_4 6 equiv. (2 equiv. 1st lot + 0.5 equiv. each in 8 lots), Pyridine, H_2O , 81%.
- Na_2CO_3 , Pyridine, CuBr , H_2O , 60%.
- 2-aminophenol 1 equiv., PPA 10 equiv., 190 °C, 24 h, 58%.
- MeI (1 equiv.), NaOH (1.05 equiv.), DMF, 80 °C, 55%

utilized which is a combination of Becke's three parameter exchange functional (B3) [32] with the nonlocal correlation functional by Lee, Yang, and Parr (LYP) [33]. The 6-31G(d) basis set [34] was employed for all atoms for the comparable exploration. To determine local minima on the energy surface of each rotamer, the vibrational frequencies for all optimized rotamers and their tautomer structures were computed using the same method [35]. The vertical excitation energies of each

rotamer at the ground state equilibrium geometries were calculated with TD-DFT [36]. The low-lying first singlet excited state of each conformer was estimated using the TD-DFT to obtain its optimized minimum energy geometry in excited state. These minimum energy geometries at excited state were used to estimate emission frequencies by TD-DFT. All the computations in solvents of different polarities were carried out using the Polarizable Continuum Model (PCM) [37, 38].

Fig. 1 Rotameric and tautomeric species of bis-2,5-(2-benzoxazolyl) hydroquinone



All electronic structure computations were carried out using the Gaussian 09 program [39] running on GridChem [40].

Result and Discussion

Compound 4

2,5-Bis(benzo[d]oxazol-2-yl)benzene-1,4-diol contains two hydroxyl groups at one and four position with respect to benzoxazole ring has two acidic protons. These acidic protons are in close vicinity of the two benzoxazole rings which leads to the possibility of various interconvertible conformational isomers arising from rotamerism and tautomerism. The possible conformers of the compound 4 with their respective keto tautomers were optimized by using B3LYP functional and 6-31G (d) basis set to determine the most stable low energy conformer. All the possible conformers of the compound 4 in enol-keto form are represented in Fig. 1. These conformers can co-exist with each other and with their tautomers in solution depending upon their relative energy difference. Relative energy difference of the different planar conformers and their tautomeric structures (Fig. 1) optimized in vapour phase by using B3LYP/6-31G (d) is given in Table 1. Enol–Keto tautomer of rotamer R1 where both hydroxyl groups are in close vicinity of N = C bond where acidic proton can have intermolecular hydrogen bond with basic nitrogen atom ($\text{OH}\cdots\text{N}=\text{C}$) is thermodynamically most stable according to B3LYP/6-31G (d) calculations in all polar and non-polar solvents. DFT calculation showed that in all the solvents keto form is less stable than the enol form due to higher energy which indicates keto is not a preferred geometry at ground state.

The thermodynamically most stable optimized structure of Compound 4 in its enol- keto form is illustrated in Fig. 2. The rotamer R1 on photo-excitation shows redistribution of charge densities which gives rise to different geometries in the

excited state. The change in bond distance and bond angle in DMF leading to the formation of excited state keto which contributes to the major red shifted emission peak is represented in Table 2. Mulliken charges on N31, H34, and O33 of the ground and excited state optimized geometries of the enol form as well as the excited state geometry of keto form are given in Table S1 (supporting data) respectively. Molecular planarity of R1 rotamer plays a significant role in ES IPT facilitating the proton transfer in the excited state from O33 to N31. In the case of DMF N31 to H34 hydrogen bonding distance decreases by 0.089 Å from Enol (1.793 Å) to Enol* (1.704 Å) while the distance between H34 and O33 was increased by 0.019 Å from Enol to Enol*, respectively. This suggests that in excited state (Enol*) the H34 approaches near to the N31 via hydrogen bonding for transfer of proton to enable ES IPT. The bond distance C4–C20 decreases from Enol (1.449 Å) to Enol* (1.415 Å) by 0.034 Å while O33–C5 bond distance decreases by 0.023 Å from Enol (1.354 Å) to Enol* (1.331 Å), which is further decreased by 0.062 Å in case of Keto* (1.269 Å). In addition to this, the bond angle H34–O33–C5 increases by 0.5° from Enol (108.5°) to Enol* (109.0°). In this way, H34 approaches nearer to N31 in Enol* and further transfer to N31 leads to Keto* with N31–H34 bond distance 1.025 Å and O33–H34 hydrogen bonding distance of 1.911 Å. The Keto* returns to ground state Keto conformer with N31–H34 bond distance of 1.045 Å and O33–H34 hydrogen bonding distance of 1.718 Å. As H34 approaches to O33 the Keto* hydrogen bonding distance decreases by 0.193 Å from 1.911 to 1.718 and it immediately converts to the Keto conformer and then to the Enol.

Photo-Physical Data for Compound 4

Photo-physical interaction of the compound 4 is represented in Table 3. Compound 4 is sensitive to solvent polarity which absorbs at 419 nm in *n*-hexane shows very slight hypsochromic shift with increase in solvent polarity and absorbs at 407 nm in DMF. In *n*-hexane it shows five absorption maxima at 419 nm, 389 nm, 333 nm, 320 nm and 304 nm which are in good agreement with the reported values 414 nm, 392 nm, 335 nm, 319 nm and 305 nm [26]. There is a good agreement with theoretical vertical excitation values obtained from TD-DFT/B3LYP 6-31G (d) calculations. A similar trend is observed in case of other non-polar and polar solvents. The largest difference in wavelength between the computed and experimental absorption maxima was 7 nm in heptane with 2.3 % deviation. In all the solvents, the prominent intense absorption can be assigned to HOMO to LUMO, HOMO to LUMO +1 and HOMO to LUMO +2 transitions of R1-enol rotamer. The frontier molecular orbital (FMO) 89 is HOMO and FMO 90 is LUMO in all the cases. The two benzoxazole rings act as an acceptor which upon excitation undergo

Table 1 Relative energies (kJ/mol) of the different planar conformers of compound 4 and their tautomeric structures in the gas phase

Rotamer	Compound 4 (Enol) (kJ/mol)	Compound 4 (Keto) (kJ/mol)
R1	0.00	0.00
R2	25.71	26.24
R3	50.55	97.98
R4	49.09	0.00
R5	96.46	45.88
R6	91.32	120.05
R7	86.05	119.81
R8	46.66	44.78
R9	91.32	44.78

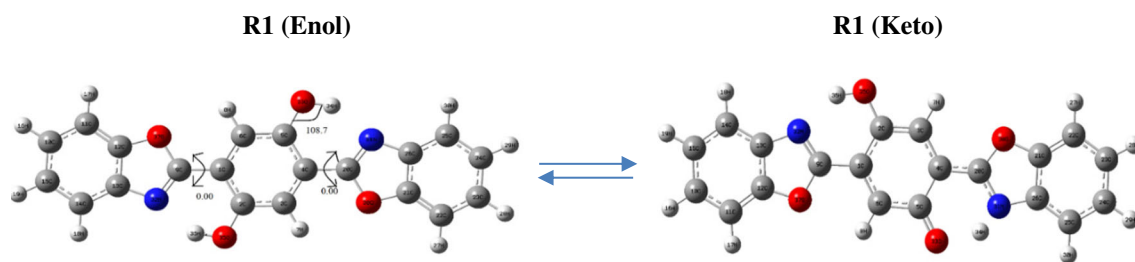


Fig. 2 Optimized structure of most stable isomer of compound 4 in DMF

HOMO to LUMO transition by the migration of electron towards one of the electron withdrawing benzoxazole ring. The electron density is mainly distributed on phenyl ring and two 1,4-hydroxy groups attached to phenyl ring in HOMO. On excitation to the LUMO, the electron density is redistributed on two benzoxazole rings which all are in one plane at excited state. Figure 3 represents the orbital distribution of electron density of compound 4 in chloroform. HOMO-LUMO electronic transition (98.7 %) for vertical excitation situated at 418 nm with oscillator strength (f) 0.6958 (Fig. 3), which corresponds to the experimentally observed absorption 410 nm with 1.95 % deviation. The HOMO to LUMO +1 (97.7 %) transition is responsible for the vertical excitation at 336 nm with oscillator strength (f) 0.9387, which corresponds to the experimentally observed absorption peak at 335 nm with 0.3 % deviation whereas HOMO to LUMO +2 (89.9) electronic transition appears at 301 nm, which corresponds to experimentally observed absorption peak at 304 nm with 0.99 % deviation. In polar solvents also similar trend is observed. This confirms that the experimentally observed short wavelength absorption in the range 304–307 nm is due to the HOMO to LUMO +2 and 333–337 nm is due to HOMO to LUMO +1 transition whereas longer wavelength absorption in the range of 404–414 nm is due to HOMO-LUMO transition.

The solvatofluorism study reveals that compound 4 shows three emissions in all polar and non-polar solvents. The long wavelength emission in all ESIPT molecules is due to the excited state keto tautomer obtained due to migration of acidic proton to basic nitrogen atom in enol excited state. The proton transfer occurs due to extra stabilization of the keto tautomer at the excited state than excited enol tautomer which is confirmed by computational calculations. The energy of excited keto form obtained from TD-DFT is lower than corresponding excited enol state in solvents, this suggest that the stabilization is solely intrinsic. TD-DFT calculation reveals that the longer wavelength emission in the range 606–631 nm is due to LUMO-HOMO transition from excited state keto to ground state keto in all solvents which corresponds with the observed emissions in the range 604–619 nm with 1.94 % of maximum deviation. Usually ESIPT compounds show single shorter wavelength emission in polar solvents attributing to LUMO-HOMO transition from excited state enol to ground state enol suggesting the exclusive presence of enol state. In case of compound 4 longer wavelength emission is also observed in polar solvents irrespective of polarity of solvents. This suggests the presence of keto tautomer in polar solvents which is further confirmed by lower energies of excited state keto conformers over respective excited state enol conformer (Supporting data Table S2). The second emission of

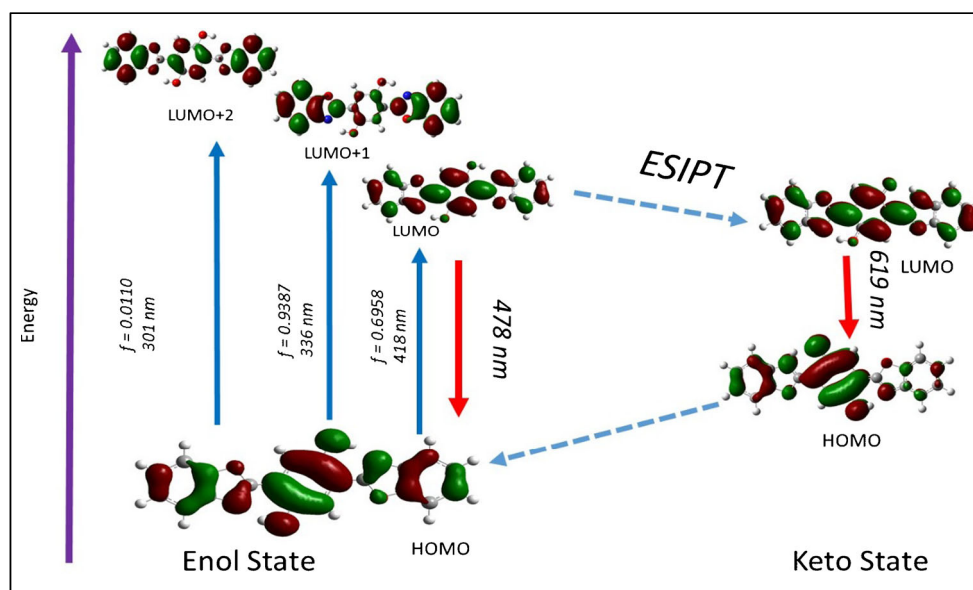
Table 2 Structural parameters of conformer R1 of compound 4 obtained by optimizing at B3LYP/6-31G(d) in DMF

		Enol E ₀	Enol E ₁	Keto K ₀	Keto K ₁
Bond Length (in Å)	N31- H34	1.793	1.704	1.045	1.025
	H34-O33	0.991	1.010	1.718	1.911
	O33-C5	1.354	1.331	1.280	1.269
	C5-C4	1.423	1.459	1.457	1.477
	C4-C20	1.449	1.415	1.410	1.410
	C20-N31	1.310	1.337	1.340	1.352
	Bond Angle (in °)	N31-H34-O33	146.0	148.4	134.0
H34-O33-C5		108.5	109.0	106.1	108.8
O33-C5-C4		123.2	120.9	123.4	120.9
C5-C4-C20		119.2	119.0	116.6	118.7
C4-C20-N31		71.126.1	126.2	125.0	127.6
C20-N31-H34		97.0	96.4	114.8	117.8

Table 3 Observed UV-visible photo-physical data and computed photo-physical data of compound 4 in different solvents

Solvent	Experimental		Theoretical				
	λ_{abs} nm	λ_{em} nm	Vertical Excitation			Emission	
			nm (Oscillator Strength)	Orbital Contribution	%D		%D
n-Hexane	419 (414)	619	422 (R1-Enol) H \rightarrow L (0.6328)	98.80	1.93	631 (R1-Keto) L \rightarrow H (0.3024)	1.93
	389 (392)	458				483 (R1-Enol) L \rightarrow H (0.5834)	5.45
	333 (335)	434	335(R1-Enol) H \rightarrow L + 1 (0.9900)	97.7	0.60		
	320 (319)						
	304 (305)		300(R1-Enol) H \rightarrow L + 2(0.0125)	79.6	1.32		
Heptane	416 (414)	617 (621)	422 (R1-Enol) H \rightarrow L (0.6370)	98.8	1.44	631(R1-Keto) L \rightarrow H (0.3042)	2.26
	389 (392)	458 (456)				483(R1-Enol) L \rightarrow H (0.5879)	5.45
	336 (335)	434 (440)	335(R1-Enol) H \rightarrow L + 1 (0.9900)	97.7	0.30		
	327 (316)						
	307 (304)		300 (R1-Enol) H \rightarrow L + 2 (0.0212)	80.2	2.28		
Chloroform	410	612	418(R1-Enol) H \rightarrow L (0.6958)	98.7	1.95	619 (R1-Keto) L \rightarrow H (0.3300)	1.11
	390	451				478 (R1-Enol) L \rightarrow H (0.6773)	5.98
	335	439	336(R1-Enol) H \rightarrow L + 1 (0.9387)	97.7	0.30		
	322						
	304		301(R1-Enol) H \rightarrow L + 2 (0.0110)	89.9	0.99		
Methanol	409	608	413(R1-Enol) H \rightarrow L (0.6987)	98.6	0.98	605 (R1-Keto) L \rightarrow H (0.3325)	0.49
	389	451				472 (R1-Enol) L \rightarrow H (0.7089)	4.6
	333	433	335(R1-Enol) H \rightarrow L + 1 (0.8870)	97.4	0.60		
	321						
	304		302(R1-Enol) H \rightarrow L + 2 (0.0089)	91.6	0.66		
DMF	407 (408)	604	414(R1-Enol) H \rightarrow L (0.7281)	98.1	1.47	609 (R1-Keto) L \rightarrow H (0.3454)	0.82
	391 (390)	455				474 (R1-Enol) L \rightarrow H (0.7404)	4.1
	337 (338)	432	336(R1-Enol) H \rightarrow L + 1 (0.8929)	97.5	0.30		
	320 (322)						
	307 (308)		302(R1-Enol) H \rightarrow L + 2 (0.0134)	92.7	1.63		
DMSO	408	604	414(R1-Enol) H \rightarrow L (0.7281)	98.7	1.47	608 (R1-Keto) L \rightarrow H (0.3444)	0.66
	389	456				474 (R1-Enol) L \rightarrow H (0.7390)	3.9
	337	432	336(R1-Enol) H \rightarrow L + 1 (0.8906)	97.5	0.30		
	319						
	304		302(R1-Enol) H \rightarrow L + 2 (0.0168)	92.6	0.66		

Fig. 3 Excited State Intramolecular Proton Transfer (ESIPT) pathway in chloroform: The vertical excitation related calculations were based on optimized ground state geometry and the emission based calculations were based on optimized excited state geometry at B3LYP/6-31G (d). The HOMO and LUMO energy levels in the excited state are different from those in the ground state. The FMO involved in the vertical excitation (UV-visible absorption: Three blue lines and emission: three red lines)



compound 4 in 472–483 nm corresponds to LUMO-HOMO transition from excited state enol to ground state enol which matches with observed emission in the range of 451–458 nm with maximum deviation of 6.0 %. Whereas third observed emission in the range of 432–439 nm may be a vibronic emission from enol excited state to enol ground state.

Compound 5

2,5-bis(benzoxazol-2-yl)-4-methoxyphenol (compound 5) has one acidic proton and one methyl group in close vicinity of two benzoxazole rings which leads to the possibility of various interconvertible conformers. All the possible conformers of the compound 5 in their enol and keto forms (illustrated in Fig. 4) are optimized by using B3LYP functional and 6-31G (d) basis set to determine the most stable low energy conformer. The relative energies of the different planar rotameric and tautomeric structures (Fig. 4) optimized in the ground and first excited states by using B3LYP/6-31G (d) are given in Table 4.

DFT optimized rotamer R16 among all sixteen rotamer is thermodynamically most stable rotamer. The optimized enol-keto geometry of stable conformer R16 in DMF is replicated in Fig. 5 along with structural parameters are tabulated in Table 5. In R16 the hydroxyl group is in vicinity of N = C bond of one the bezoxazole ring to felicitate intramolecular hydrogen bond formation with basic nitrogen atom ($\text{OH} \cdots \text{N} = \text{C}$) and methyl group is moving away from other benzoxazole ring to minimise the steric hindrance.

Change in Mullikan charges on N31, H34, and O33 atom of compound 5 in ground and excited of Keto-Enol tautomer of R16 is given Table S3 (Supporting data). The most stable rotamer R16 of compound 5 shows complete planarity in a

region where hydrogen from O33-H34 is in close vicinity of N31. The planarity in this region promotes proton transfer upon photo excitation. The change in bond distance in optimized keto-enol tautomeric structures proves the successful transfer of acid proton H34 on photo excitation. The bond distance between N31- H34 decreases by 0.065 Å from Enol (1.797 Å) to Enol* (1.732 Å) whereas the distance between H34 -O33 was enhanced by 0.013 Å from Enol to Enol* suggesting the approach of H34 to N31 via hydrogen bonding for transfer of proton during photo excitation. The decrease in bond distances C4-C20, and O33-C5 from Enol to Enol* and further decrease from Enol* to Keto* confirms the possibility of ESIPT upon absorption of light. In addition to this, the bond angle H34-O33-C5 increases by 0.4° from Enol (108.4°) to Enol* (108.9°). The H34 approaches nearer to N31 in Enol* and further transfer to N31 to give Keto* with N31-H34 bond distance 1.027 Å and O33-H34 hydrogen bonding distance of 1.904 Å. The Keto* returns to ground state Keto conformer with N31-H34 bond distance of 1.040 Å and O33-H34 hydrogen bonding distance of 1.748 Å.

Photo-Physical Data for Compound 5

Table 6 shows the interaction of compound 5 with light in presence of different solvents. Compound 5 shows sensitivity to solvent polarity and shows negative solvatochromism and positive solvatofluorism from non-polar to polar solvent. It shows absorption at 402 nm in *n*-Hexane whereas in case of DMSO the absorption peak was observed at 380 nm. In comparison with compound 4 introduction of methyl group in compound 5 shows blue shift in absorption maxima in all solvents as well as it shows only three prominent absorption peak in all the solvents. The ratio of intensity of three

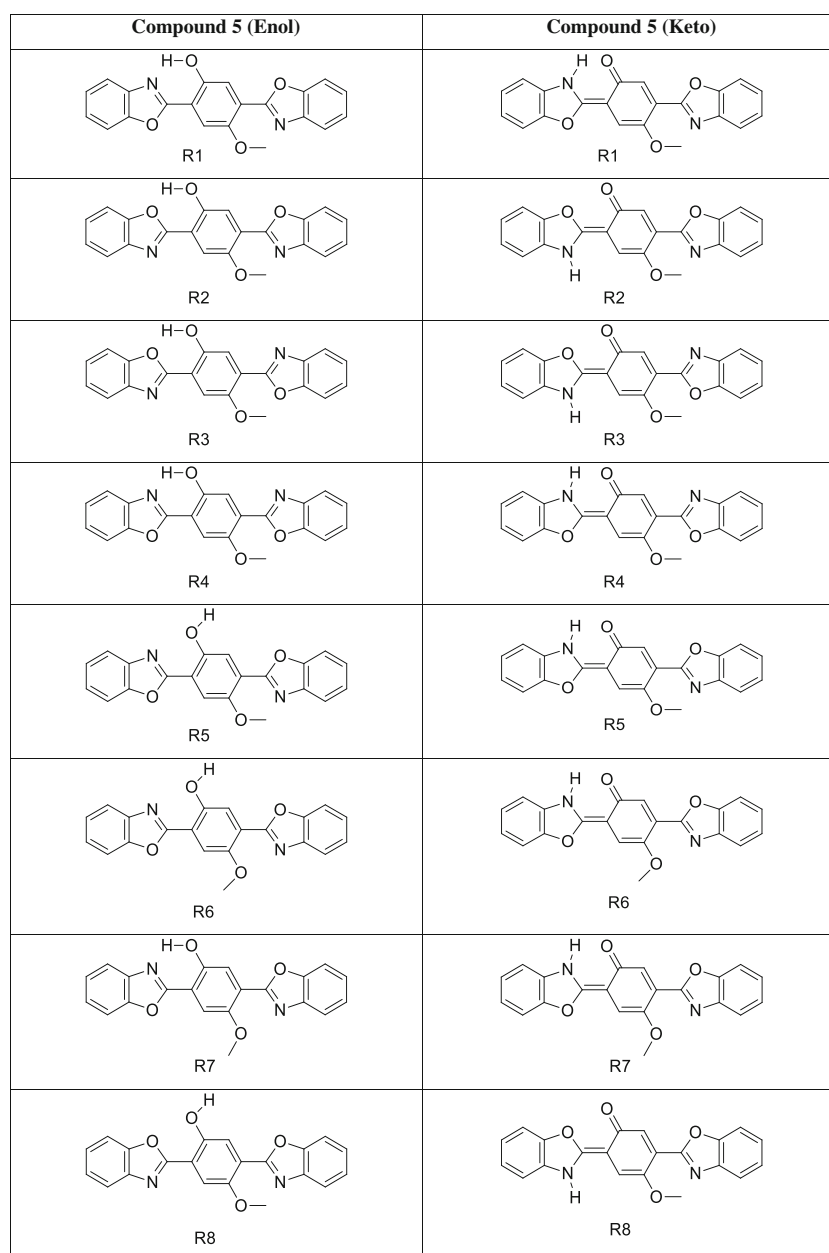


Fig. 4 Different possible Enol-Keto conformers of compound 5

absorption peaks remains almost constant in all the solvents. In heptane it shows absorption maxima at 402 nm, 378 nm, 318 nm which are in good agreement with the reported values 308 nm, 376 nm, 315 nm [28]. The theoretical values obtained from vertical excitation using TD-DFT/B3LYP 6-31G (d) calculations show very good agreement with observed values in all solvents. The maximum deviation in theoretical vertical excitation from observed value is 10 % observed in n-hexane.

In all the solvents, the prominent intense absorption can be assigned to HOMO to LUMO, HOMO to LUMO + 1 and HOMO to LUMO + 2 transitions of R16-enol rotamer. The

frontier molecular orbital (FMO) 93 is HOMO and FMO 94 is LUMO in all the cases. The two benzoxazole rings act as an acceptor which upon excitation undergo HOMO to LUMO transition. The electron density is mainly distributed on phenyl ring along with hydroxyl and methoxy group attached to phenyl ring in HOMO. On excitation the electron density is redistributed on two benzoxazole rings which all are in one plane at excited state. Fig S1 (Supporting data) represents the orbital distribution of electron density of compound 5 in chloroform. HOMO-LUMO electronic transition (98.4 %) for vertical excitation situated at 406 nm with oscillator strength (f)

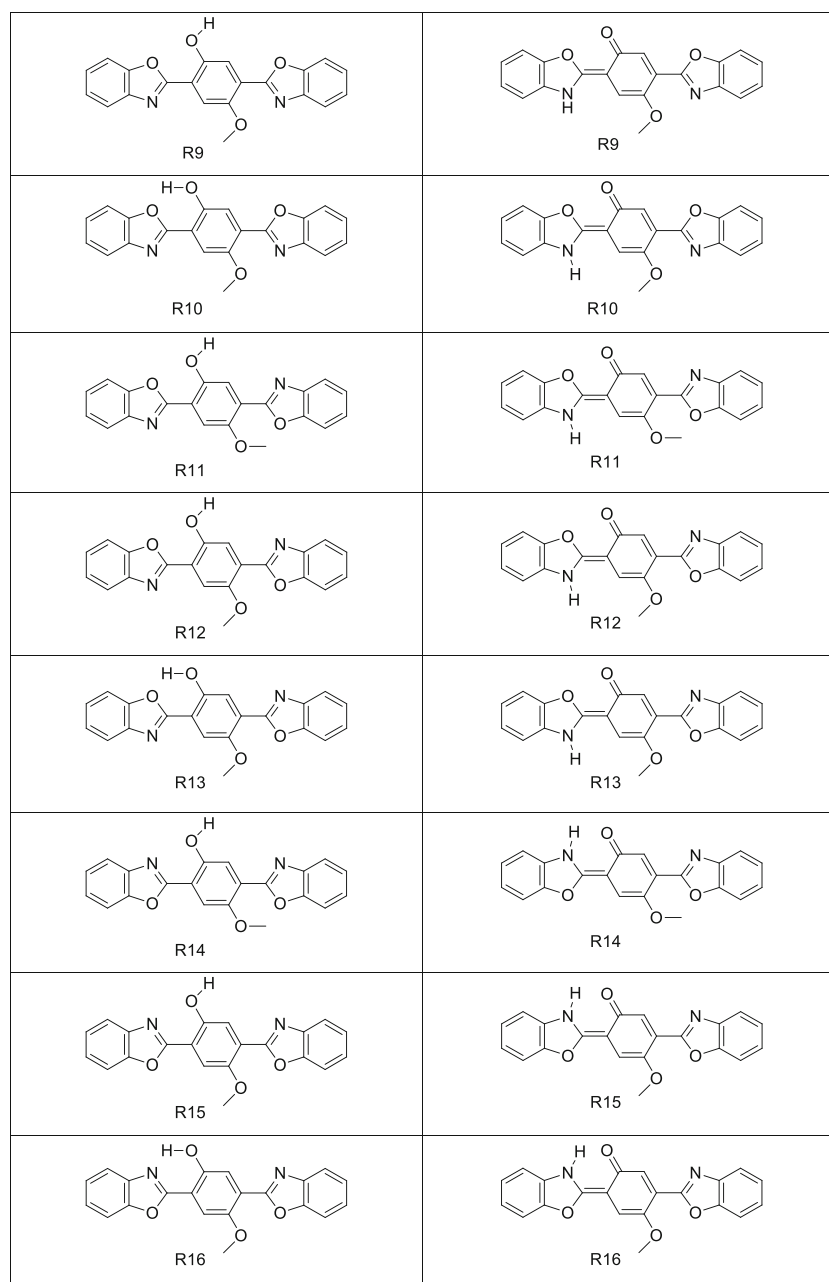


Fig. 4 (continued)

0.8897 (Fig. 3), which corresponds to the experimentally observed absorption 383 nm with 6.0 % deviation. The HOMO to LUMO + 1 (97.0 %) transition is responsible for the vertical excitation at 340 nm with oscillator strength (f) 0.6565, which corresponds to the experimentally observed absorption peak at 368 nm with 7.6 % deviation whereas HOMO to LUMO + 2 (89.9) electronic transition appears at 305 nm, which corresponds to experimentally observed absorption peak at 320 nm with 4.6 % deviation. In polar solvents also similar trend is observed. This confirms that the experimentally observed

short wavelength absorption in the range 317–320 nm is due to the HOMO to LUMO + 2 and 361–379 nm is due to HOMO to LUMO + 1 transition whereas longer wavelength absorption in the range of 380–402 nm is due to HOMO-LUMO transition.

The solvatofluorism study reveals that compound 5 shows three emissions in all polar and non-polar solvents. The longer wavelength emission is obtained due to migration of acidic proton to basic nitrogen atom in enol excited state. The proton transfer occurs due to extra stabilization of the keto tautomer

Table 4 Relative energies (KJ/mol) of the different planar conformers of compound 5 and their tautomeric structures in the gas phase

Rotamers	Compound 5 Enol (KJ/mol)	Compound 5 Keto (KJ/mol)
R1	5.60	3.26
R2	22.73	74.40
R3	22.73	74.40
R4	6.61	5.94
R5	54.89	3.26
R6	49.95	0.92
R7	1.77	0.92
R8	49.45	74.00
R9	44.99	74.00
R10	24.97	74.00
R11	49.45	78.88
R12	40.25	73.84
R13	22.73	73.87
R14	53.11	5.94
R15	45.59	0.00
R16	0.00	0.00

at the excited state than excited enol tautomer which is confirmed by computational calculations. Compound 5 shows red shift in emission from non-polar to polar solvents. In n-hexane it emits at 560 nm where as in DMSO emission maximum is at 582 nm. The longer wavelength emission in the range 560–582 nm is due to LUMO-HOMO transition from excited state keto to ground state keto in all solvents which corresponds to theoretical emissions range 553–562 nm with 4.3 % of maximum deviation. The longer wavelength emission in compound 5 in all solvents show a blue shift in comparison with compound 4 where emission range is 604–619 nm in all solvents. Usually ESIPT compounds show single shorter wavelength emission in polar solvents attributing to LUMO-HOMO transition from excited state enol to ground state enol suggesting the exclusive presence of enol state. In case of compound 5 like compound 4 longer wavelength emission is also observed in polar solvents irrespective of polarity of solvents. This suggests the presence of keto tautomer in polar

Table 5 Structural parameters of conformer R16 of compound 5 obtained by optimizing at B3LYP/6-31G(d) in DMF

		Enol E ₀	Enol E ₁	Keto K ₀	Keto K ₁
Bond Length (in Å)	N31-H34	1.797	1.732	1.040	1.027
	H34-O33	0.991	1.004	1.748	1.904
	O33-C5	1.353	1.337	1.276	1.271
	C5-C4	1.416	1.457	1.452	1.476
	C4-C20	1.447	1.411	1.407	1.409
	C20-N31	1.310	1.338	1.341	1.353
Bond Angle (in °)	N31-H34-O33	145.9	148.2	132.8	126.8
	H34-O33-C5	108.4	108.9	106.0	108.7
	O33-C5-C4	123.4	121.0	123.7	120.7
	C5-C4-C20	119.4	119.5	116.9	118.9
	C4-C20-N31	126.1	126.5	125.3	127.5
	C20-N31-H34	96.9	96.0	115.3	117.4

solvents which is further confirmed by lower energies of excited state keto conformers over respective excited state enol conformer Table S4 (Supporting data). The second observed emission of compound 5 in 438–442 nm range corresponds to LUMO-HOMO transition from excited state enol to ground state enol which matches with theoretical emission in the range of 456–461 nm obtained from TD-DFT calculations with maximum deviation of 4.3 %. Whereas third emission obtained in the range of 413–420 nm is may a vibronic emission obtained from enol excited state to enol ground state.

Conclusions

To conclude, this paper reports the structural parameters of most stable conformer obtained from DFT calculation considering all possible rotamers of bis-2,5-(2-benzoxazolyl) hydroquinone and 2,5-bis (benzo[d]oxazol-2-yl)-4-methoxyphenol. The photo-physical behaviour of these compounds in six different solvents was determined which is in very good agreement with previously reported values for some of the solvents. The vertical excitation and emission determined by using the

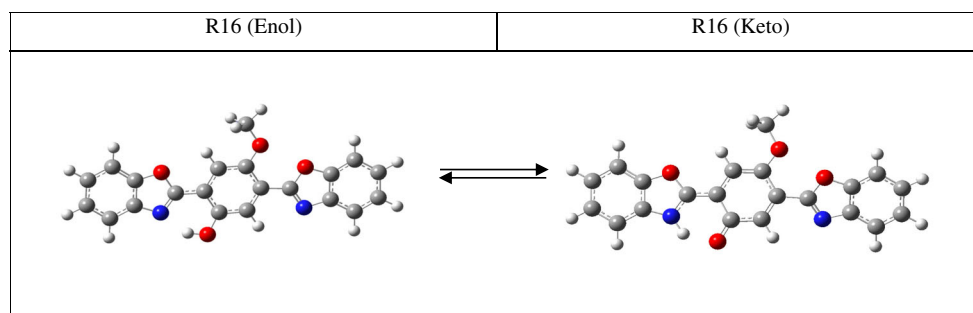
Fig. 5 Optimized structure of most stable isomer of compound 5 in DMF

Table 6 Observed UV-visible photo-physical data and computed photo-physical data of compound 5 in different solvents

Solvent	Experimental		Theoretical				
	λ_{abs} nm	λ_{em} nm	Vertical Excitation			Emission	
			nm (Oscillator Strength)	Orbital Contribution	%D	nm (Oscillator Strength)	%D
n-Hexane	402(399)	560	405 (R16-Enol) H \rightarrow L (0.8644)	98.3	0.7	553 (R16-Keto) L \rightarrow H (0.3527)	1.2
	379(375)	438	341 (R16-Enol) H \rightarrow L + 1 (0.6327)	97.0	10.0	456 (R16-Enol) L \rightarrow H (0.0.8973)	4.1
	318(315)	413	305 (R16-Enol) H \rightarrow L + 2 (0.0594)	88.63	4.0		
Heptane	402(398)	569(571)	405 (R16-Enol) H \rightarrow L (0.8686)	98.3	0.7	554 (R16-Keto) L \rightarrow H (0.3591)	2.6
	378(376)	439(438)	341 (R16-Enol) H \rightarrow L + 1 (0.6333)	97.0	9.8	456 (R16-Enol) L \rightarrow H (0.9032)	3.9
	318(315)	412(414)	305 (R16-Enol) H \rightarrow L + 2 (0.0600)	88.4	4.0		
Chloroform	383	580	406 (R16-Enol) H \rightarrow L (0.8897)	98.4	6.0	559 (R16-Keto) L \rightarrow H (0.3764)	3.6
	368	440	340 (R16-Enol) H \rightarrow L + 1 (0.6565)	97.0	7.6	460 (R16-Enol) L \rightarrow H (0.9828)	4.5
	320	415	305 (R16-Enol) H \rightarrow L + 2 (0.0723)	81.3	4.6		
Methanol	382	582	404 (R16-Enol) H \rightarrow L (0.8548)	98.2	5.7	558 (R16-Keto) L \rightarrow H (0.3687)	4.1
	365	441	338 (R16-Enol) H \rightarrow L + 1 (0.6721)	96.8	7.3	459 (R16-Enol) L \rightarrow H (0.9821)	4.1
	318	416	305 (R16-Enol) H \rightarrow L + 2 (0.0623)	85.0	4.0		
DMF	383 (381)	585	406 (R16-Enol) H \rightarrow L (0.8883)	98.3	6.0	562 (R16-Keto) L \rightarrow H (0.3834)	4.0
	362	441	339 (R16-Enol) H \rightarrow L + 1 (0.6737)	97.0	6.3	462 (R16-Enol) L \rightarrow H (1.0211)	4.8
	320 (318)	417	305 (R16-Enol) H \rightarrow L + 2 (0.0629)	87.3	4.6		
DMSO	380	586	405 (R16-Enol) H \rightarrow L (0.8843)	98.3	6.5	561 (R16-Keto) L \rightarrow H (0.3820)	4.3
	361	442	339 (R16-Enol) H \rightarrow L + 1 (0.6741)	97.0	6.1	461 (R16-Enol) L \rightarrow H (1.0175)	4.3
	317	420	305 (R16-Enol) H \rightarrow L + 2 (0.0621)	87.3	3.8		

Density Functional Theory (DFT) and Time-Dependent Density Functional Theory (TD-DFT). Compound 4 shows five absorption and three emission peaks in all the solvents whereas compound 5 shows three absorption and three emission peaks. The photo physical properties of the compounds are sensitive towards the solvent environment. Compound 4 shows red shift in absorption and emission in comparison with compound 5. Photo physical properties of the compounds were supported by DFT and it was observed that computational results are good agreement with the theoretical observations.

Acknowledgments The Author, Manoj M. Jadhav is grateful to Department of Science and Technology (DST) and Technical Education Quality Improvement Programme (TEQIP) for financial assistance.

References

1. Chou P-T, Huang, Pu S-C, et al. (2004) Tuning excited-state charge/proton transfer coupled reaction via the dipolar functionality. *J Phys Chem A* 108:6452–6454. doi:10.1021/jp0476390
2. Banerjee C, Maiti S, Mustafi M, et al. (2014) Effect of encapsulation of curcumin in polymeric nanoparticles: how efficient to control ESIPT process? *Langmuir* 30:10834–10844. doi:10.1021/la5023533
3. Patil VS, Padalkar VS, Phatangare KR, et al. (2012) Synthesis of new ESIPT-fluorescein: photophysics of pH sensitivity and fluorescence. *J Phys Chem A* 116:536–545. doi:10.1021/jp2073123
4. Song Z, Kwok RTK, Zhao E, et al. (2014) A ratiometric fluorescent probe based on ESIPT and AIE processes for alkaline phosphatase activity assay and visualization in living cells. *ACS Appl Mater Interfaces* 6:17245–17254. doi:10.1021/am505150d

5. Chung M-W, Lin T-Y, Hsieh C-C, et al. (2010) Excited-state intramolecular proton transfer (ESIPT) fine tuned by quinoline – pyrazole isomerism: π -conjugation effect on ESIPT. *J Phys Chem A* 114: 7886–7891. doi:10.1021/jp1036102
6. Lim S-J, Seo J, Park SY (2006) Photochromic switching of excited-state intramolecular proton-transfer (ESIPT) fluorescence: a unique route to high-contrast memory switching and nondestructive read-out. *J Am Chem Soc* 128:14542–14547. doi:10.1021/ja0637604
7. Phatangare KR, Gupta VD, Tathe AB, et al. (2013) ESIPT inspired fluorescent 2-(4-benzo[d]oxazol-2-yl)naphtho[1,2-d]oxazol-2-yl)phenol: experimental and DFT based approach to photophysical properties. *Tetrahedron* 69:1767–1777. doi:10.1016/j.tet.2012.11.095
8. Roberts EL, Chou PT, Alexander TA, et al. (1995) Effects of organized media on the excited-state intramolecular proton transfer of 10-Hydroxybenzo[h]quinoline. *J Phys Chem* 99:5431–5437. doi:10.1021/j100015a028
9. Abou-Zied OK, Jimenez R, Thompson EH, et al. (2002) Solvent-dependent photoinduced tautomerization of 2-(2'-Hydroxyphenyl)benzoxazole. *J Phys Chem A* 106:3665–3672. doi:10.1021/jp013915o
10. Seo J, Kim S, Park SY (2004) Strong solvatochromic fluorescence from the intramolecular charge-transfer state created by excited-state intramolecular proton transfer. *J Am Chem Soc* 126:11154–11155. doi:10.1021/ja047815i
11. Stephan JS, Rodríguez CR, Grellmann KH, Zachariasse KA (1994) Flash-photolysis of 2-(2'-hydroxyphenyl)-3-H-indole. Ground-state keto-enol tautomerization by mutual hydrogen exchange and by proton catalysis. *Chem Phys* 186:435–446. doi:10.1016/0301-0104(94)01624-0
12. Park S, Kwon O-H, Kim S, et al. (2005) Imidazole-based excited-state intramolecular proton-transfer materials: synthesis and amplified spontaneous emission from a large single crystal. *J Am Chem Soc* 127:10070–10074. doi:10.1021/ja0508727
13. Holler MG, Campo LF, Brandelli A, Stefani V (2002) Synthesis and spectroscopic characterisation of 2-(2'-hydroxyphenyl)benzazole isothiocyanates as new fluorescent probes for proteins. *J Photochem Photobiol A Chem* 149:217–225. doi:10.1016/S1010-6030(02)00008-4
14. Yan L, Ye Z, Peng C, Zhang S (2012) A new perylene diimide-based fluorescent chemosensor for selective detection of ATP in aqueous solution. *Tetrahedron* 68:2725–2727. doi:10.1016/j.tet.2012.01.028
15. Rodríguez JG, Tejedor JL (2005) Carbon dendron nano-chains with π -extended conjugation based on end-capped N,N-dimethylamino in linear 1,4-phenylethynyl or in 1,5-naphthylethynyl subunits: fluorescence analysis. *Tetrahedron* 61:2047–2054. doi:10.1016/j.tet.2004.12.054
16. Tang K-C, Chang M-J, Lin T-Y, et al. (2011) Fine tuning the energetics of excited-state intramolecular proton transfer (ESIPT): white light generation in a single ESIPT system. *J Am Chem Soc* 133: 17738–17745. doi:10.1021/ja2062693
17. Paterson MJ, Robb MA, Blancafort L, DeBellis AD (2005) Mechanism of an exceptional class of photostabilizers: a seam of conical intersection parallel to excited state intramolecular proton transfer (ESIPT) in o-Hydroxyphenyl-(1,3,5)-triazine. *J Phys Chem A* 109:7527–7537. doi:10.1021/jp051108+
18. Kim S, Park SY, Yoshida I, et al. (2002) Amplified spontaneous emission from the film of poly(aryl ether) dendrimer encapsulating excited-state intramolecular proton transfer dye. *J Phys Chem B* 106:9291–9294. doi:10.1021/jp021048x
19. Kim CH, Park J, Seo J, et al. (2010) Excited state intramolecular proton transfer and charge transfer dynamics of a 2-(2'-Hydroxyphenyl)benzoxazole derivative in solution. *J Phys Chem A* 114:5618–5629. doi:10.1021/jp909438p
20. Chen W, Twum EB, Li L, et al. (2012) Rotational energy barrier of 2-(2',6'-Dihydroxyphenyl)benzoxazole: a case study by NMR. *J Org Chem* 77:285–290. doi:10.1021/jo201890f
21. Davidson JP, Corey EJ (2003) First enantiospecific total synthesis of the antitubercular marine natural product pseudopteroxazole. Revision of assigned stereochemistry. *J Am Chem Soc* 125: 13486–13489. doi:10.1021/ja0378916
22. Leaver IH, Milligan B (1984) Fluorescent whitening agents—a survey (1974–82). *Dyes Pigments* 5:109–144. doi:10.1016/0143-7208(84)80008-X
23. Stefani V, Souto AA, Acuña AU, Amat-Guerri F (1992) Synthesis of proton-transfer fluorescent dyes: 2,5-bis(2'-benzazolyl)hydroquinones and related compounds. *Dyes Pigments* 20:97–107. doi:10.1016/0143-7208(92)85003-5
24. Mordziński A, Grabowska A, Kühnle W, Kröwczynski A (1983) Intramolecular single and double proton transfer in benzoxazole derivatives. *Chem Phys Lett* 101:291–296. doi:10.1016/0009-2614(83)87015-8
25. Cosnier S, Deronzier A, Moutet JC (1985) Photoresponse of platinum electrodes coated by electropolymerized polypyridyl complexes of ruthenium(II)-containing pyrrole groups in the presence of an external quencher. Film thickness effect. *J Phys Chem* 89: 4895–4897. doi:10.1021/j100269a001
26. Grabowska A, Sepiol J, Rulliere C (1991) Mechanism and kinetics of proton-transfer reactions in excited, internally hydrogen-bonded benzoxazole derivatives as studied by picosecond transient absorption and stimulated emission pumping. *J Phys Chem* 95:10493–10495. doi:10.1021/j100178a041
27. Mordziński A, Kuehnle W (1986) Kinetics of excited-state proton transfer in double benzoxazoles: 2,5-bis(2-benzazolyl)-4-methoxyphenol. *J Phys Chem* 90:1455–1458. doi:10.1021/j100398a047
28. Ernsting NP (1985) Dual fluorescence and excited-state intramolecular proton transfer in jet-cooled 2,5-bis(2-benzazolyl)hydroquinone. *J Phys Chem* 89:4932–4939. doi:10.1021/j100269a010
29. Chen Y-C, Yu C-Y, Fan Y-L, et al. (2010) Low-bandgap conjugated polymer for high efficient photovoltaic applications. *Chem Commun* 46:6503–6505. doi:10.1039/C0CC01087A
30. Chen SH, Wong KT, Lin YY, et al. (2010) Diindenothiophene derivatives and use thereof, US 20100168444 A1
31. Treutler O, Ahlrichs R (1995) Efficient molecular numerical integration schemes. *J Chem Phys* 102:346–354
32. Becke AD (1993) A new mixing of Hartree–Fock and local density-functional theories. *J Chem Phys* 98:1372–1377
33. Lee C, Yang W, Parr RG (1988) Development of the Colle–Salvetti correlation-energy formula into a functional of the electron density. *Phys Rev B* 37:785–789. doi:10.1103/PhysRevB.37.785
34. Casida ME, Jamorski C, Casida KC, Salahub DR (1998) Molecular excitation energies to high-lying bound states from time-dependent density-functional response theory: characterization and correction of the time-dependent local density approximation ionization threshold. *J Chem Phys* 108:4439–4349
35. Li H, Niu L, Xu X, et al. (2011) A comprehensive theoretical investigation of intramolecular proton transfer in the excited states for some newly-designed diphenylethylene derivatives bearing 2-(2-Hydroxy-Phenyl)-Benzotriazole part. *J Fluoresc* 21:1721–1728. doi:10.1007/s10895-011-0867-6
36. Bauernschmitt R, Ahlrichs R (1996) Treatment of electronic excitations within the adiabatic approximation of time dependent density functional theory. *Chem Phys Lett* 256:454–464. doi:10.1016/0009-2614(96)00440-X
37. Cossi M, Barone V, Cammi R, Tomasi J (1996) Ab initio study of solvated molecules: a new implementation of the polarizable continuum model. *Chem Phys Lett* 255:327–335. doi:10.1016/0009-2614(96)00349-1

38. Tomasi J, Mennucci B, Cammi R (2005) Quantum mechanical continuum solvation models. *Chem Rev* 105:2999–3094. doi:[10.1021/cr9904009](https://doi.org/10.1021/cr9904009)
39. Frisch MJ, Trucks GW, Schlegel HB, et al. (2009) Gaussian 09, Revision C.01. Gaussian 09, Revis. B.01, Gaussian, Inc., Wallingford CT
40. Dooley R, Milfeld K, Guiang C, et al. (2006) From proposal to production: lessons learned developing the computational chemistry grid cyberinfrastructure. *J Grid Comput* 4:195–208. doi:[10.1007/s10723-006-9043-7](https://doi.org/10.1007/s10723-006-9043-7)